Article

Bias-Corrected RADARSAT-2 Soil Moisture Dynamics Reveal Discharge Hysteresis at An Agricultural Watershed

Ju Hyoung Lee [1,*] and Karl-Erich Lindenschmidt [2]

[1] Department of Geography, Environment & Geomatics, University of Guelph, 50 Stone Rd E, Guelph, ON N1G 2W1, Canada

[2] Global Institute for Water Security, School of Environment and Sustainability, University of Saskatchewan, 11 Innovation Boulevard, Saskatoon, SK S7N 3H5, Canada; karl-erich.lindenschmidt@usask.ca

* Correspondence: lee06@uoguelph.ca; Tel./Fax: +1-519-824-4120

Abstract: Satellites are designed to monitor geospatial data over large areas at a catchment scale. However, most of satellite validation works are conducted at local point scales with a lack of spatial representativeness. Although upscaling them with a spatial average of several point data collected in the field, it is almost impossible to reorganize backscattering responses at pixel scales. Considering the influence of soil storage on watershed streamflow, we thus suggested watershed-scale hydrological validation. In addition, to overcome the limitations of backscattering models that are widely used for C-band Synthetic Aperture Radar (SAR) soil moisture but applied to bare soils only, in this study, RADARSAT-2 soil moisture was stochastically retrieved to correct vegetation effects arising from agricultural lands. Roughness-corrected soil moisture retrievals were assessed at various spatial scales over the Brightwater Creek basin (land cover: crop lands, gross drainage area: 1540 km^2) in Saskatchewan, Canada. At the point scale, local station data showed that the Root Mean Square Errors (RMSEs), Unbiased RMSEs (ubRMSEs) and biases of Radarsat-2 were 0.06~0.09 m^3/m^3, 0.04~0.08 m^3/m^3 and 0.01~0.05 m^3/m^3, respectively, while 1 km Soil Moisture Active Passive (SMAP) showed underestimation at RMSEs of 0.1~0.22 m^3/m^3 and biases of $-0.036\sim-0.2080$ m^3/m^3. Although SMAP soil moisture better distinguished the contributing area at the catchment scale, Radarsat-2 soil moisture showed a better discharge hysteresis. A reliable estimation of the soil storage dynamics is more important for discharge forecasting than a static classification of contributing and noncontributing areas.

Keywords: soil moisture; RADARSAT-2; SMAP; stochastic retrievals; bias correction

1. Introduction

Soil moisture is an essential variable in the hydrological cycle. Soil moisture modulates the partitioning of rainfall into runoff and infiltration, which further determines the recharge of groundwater. Thus, to improve discharge or flooding predictions, it is important to accurately estimate or appropriately assimilate soil moisture into hydrological models [1–5]. In this context, using local station data may not resolve the major limitations of physical and conceptual rainfall runoff models, such as a lack of spatial variability of the catchment or site-dependent parameterization [6]. Wanders et al. [2] pointed out that in-situ soil moisture measurements acquired from local stations are too scarce to cover large-scale watersheds and have a lack of sufficient spatial representation of the drainage area, even when upscaled. Accordingly, the spatial distribution information of satellite-retrieved soil moisture is a key element for calibrating and validating hydrological models.

Previously, several studies have attempted to apply remote sensing data for producing hydrological maps, such as the contributing area that is referred to as the part of the basin that contributes to the surface runoff [7]. The contributing area is an essential feature to understand catchment behavior. Due to its significance in the streamflow response,

Mengistu and Spence [8] investigated a hysteretic relationship with the streamflow by using a SPOT (Satellite pour l'Observation de la Terre)-derived contributing area. However, they found that cloud shadow-free SPOT-5 images are too infrequent to characterize events-based contributing or saturated areas. The Normalized Difference Vegetation Index (NDVI) from visible or infrared sensors also has limitations when used as a proxy for landscape-scale soil moisture variation because of its low sensitivity to soil moisture. On the other hand, Gala, et al. [9] and Gala and Melesse [10] attempted to employ RADARSAT-1 SAR to map saturated and inundated areas, assuming a proportional relationship between the dielectric property and soil moisture. However, due to a nonlinear relationship between the dielectric property and soil moisture, and the technical challenge of distinguishing other physical parameters such as soil roughness from soil moisture, the application of this assumption is often limited.

In 2009, the first satellite specialized for retrieving global soil moisture was launched. The Soil Moisture and Ocean Salinity (SMOS) operates in the L-band (1.4 GHz) frequency that is sensitive to soil moisture [11]. The Soil Moisture Active Passive (SMAP) mission launched in January 2015 and also provides global estimates of soil moisture. SMAP radiometer data have been used to produce several products, including high-resolution data available at 1~3 km [12,13]. Compared to L-band microwave radiometer-based satellite missions with relatively low spatial resolution (25~40 km), Synthetic Aperture Radar (SAR) satellites provide high-resolution surface soil moisture estimates at the spatial scale of several meters. For example, various microwave sensors, including Terra SAR-X, the Advanced Land Observing Satellite (ALOS), Sentinel-1, Gaofen-3 (GF-3) and RADARSAT Constellation, are available to provide SAR data at high spatial resolutions (~100 m) in various frequencies, such as X-band (9.6 GHz), C-band (3.9–5.75 GHz) or L-band (0.39–1.55 GHz), with single, dual or full polarization [14–18].

Although several satellite measurements are available at the global scale, it is still challenging to retrieve watershed-scale soil moisture from them for various reasons. As the manner in which the radiance or backscatter interacts with natural surface conditions is so complicated and heterogeneous, it is difficult to standardize or parameterize large-scale land surfaces with models. For example, the empirical Water Cloud Model was suggested for retrieving soil moisture over crop lands with active microwave data [19]. To estimate two-way transmissivity formulated in the model, vegetation information such as the vegetation layer and vegetation optical depth is required. However, not only is this not well determined with globally available satellite data, but several site-specific and empirical parameters of vegetation structures, such as crop type or vegetation height, should also be locally calibrated [20]. We have no choice but to keep using the local estimations. Thus, it cannot be used for global maps. This limitation when using empirical models is also applicable to passive microwave retrievals that use tau-omega radiative transfer models. Hence, several studies have reported that the accuracy of soil moisture retrievals decreases with increasing the vegetation density [2].

For this reason, inversion is often used to estimate large areas. An inversion algorithm reverses physical-based radiative transfer models by conjecturing several unknown input parameters considered as model outputs from the satellite measurements. It is widely used for soil moisture retrievals, as it accommodates an ill-posed problem, meaning that it determines multiple parameters without the need for in-situ measurements or local calibrations.

However, inversion errors often occur, failing in the convergence between measurement and model estimations. Fundamentally, the relationship between satellite-measured backscatter coefficients or brightness temperature and soil moisture (i.e., dielectric constant values) is nonlinear [21,22]. Thus, it may encounter equifinality; that is, the different compositions of several parameters constitute the same satellite measurements. In addition, as suggested above, empirically or physically based models used for inversion are not able to explicitly formulate the complexity and heterogeneity of land surfaces. The surface scattering models often used for SAR inversion also assume bare or smooth surfaces without volume scattering usually from agricultural lands [14,23,24]. In addition to inversion errors,

a change detection is also hampered by a simplified assumption of roughness or vegetation. Taken together, the radiative transfer models used for an inversion or change detection usually assume a 'nominal' condition, in which the vegetation water content (VWC) is less than 5 kg/m^2; there are no urban, heavily forested, frozen or permanent snow/ice areas; the soil texture supplementary information is perfect; the effect of the soil roughness is negligible and the vegetation does not change at a low resolution [12,23,25–27]. Therefore, the retrieval algorithms used for both active and passive microwave observations are often exposed to retrieval errors [28–32].

To overcome the limitations of conventional inversions and correct the vegetation effects or roughness errors, a stochastic approach is often applied by employing a probability distribution function (PDF). In this approach, the statistical likelihood of particular parameters is considered rather than fixed values from a priori knowledge of surface parameters [33–35]. Verhoest et al. [33] defined soil roughness with a probability distribution to retrieve soil moisture from the European Remote Sensing (ERS) scatterometer. Their results showed reliable retrievals at RMSEs of less than 6%. Some studies have established the probability distribution function (PDF) by running a forward model under a broad range of conditions [34,35]. In addition to soil roughness, the PDFs are often conditioned to SAR backscatter coefficients, brightness temperature measurements, VWC or soil moisture. To take into account the effects of vegetation, Pierdicca et al. [36] inverted soil moisture with the Bayesian maximum posterior probability that maximizes the PDF of the target parameters conditioned to the measurements. The RMSE decreased while the correlations improved. To consider vegetation effects, Notarnicola et al. [37] also used a Bayesian approach by constructing PDF with the vegetation water content estimated from a Landsat image. Lee et al. [34] also mitigated retrieval errors related to rainfall and vegetation by the construction of PDFs of uncertain parameters, such as roughness or SAR backscatter measurements. These stochastic systems can be optimized by clustering analysis [38,39].

However, the retrieval bias correction suggested above cannot be replaced by data assimilation, which only considers random errors. Furthermore, the cumulative distribution function (CDF) matching utilized for satellite data assimilation is suggested to reduce the difference between in-situ measurements or model estimates and satellite retrievals, while triple collocation (TC) estimates the uncertainty among different products [40,41]. Therefore, they are not designed to have effects such as removing retrieval biases or measurement errors [42].

The objective of this study is to retrieve high-resolution roughness and soil moisture at the catchment scale from Radarsat-2 backscatter data by stochastically correcting the vegetation effects from crop lands. This study aims at evaluating which retrieval bias correction and hydrological mapping (contributing to area classification) are more important to capture watershed discharge hysteresis and to enhance runoff models. This paper is organized as follows. The study area and local measurements are briefly introduced in Sections 2.1 and 2.2. Descriptions of the Radarsat-2 data and retrieval methods are provided in Section 2.3. In Section 2.4., pure SMAP surface soil moisture without a bias correction is provided as a simple comparison of the bias-corrected Radarsat-2 retrievals. In Section 3, the results and discussions are provided from the perspectives of local point validation, spatial distribution and hydrological validation with water levels at a prairie outlet. Section 4 draws the conclusions.

2. Methods and Data

2.1. Study Area

The Brightwater Creek (BWC) watershed is located within the south river basin of Central Saskatchewan in Canada and a semi-arid region (mean annual precipitation: approximately 330 mm during 2009–2014) [7]. The mean air temperature is approximately 18–20 °C in July. As shown in Figure 1a, several soil moisture local stations are available in this region to validate and calibrate various hydrological research activities, including research associated with the Changing Cold Regions Network (CCRN) [43], in addition

to satellite missions such as the European Space Agency (ESA)'s SMOS and the National Aeronautics and Space Administration (NASA)'s Soil Moisture Active Passive (SMAP) [44]. The locations of each station are presented in Table 1 and Figure 1a. The spatial domain in Figure 1a is set to include those stations, ranging from latitude 50.8029° to 51.9298° to longitude −107.1698° to −105.5573°. The contributing and noncontributing areas delineated in Figure 1a were obtained from the PFRA (Prairie Farm Rehabilitation Administration)-Agriculture and Agri-Food Canada dataset, which was created by the flow network to track the hydrometric gauging station's upstream and downstream neighbors.

(**a**)

(**b**)

(**c**)
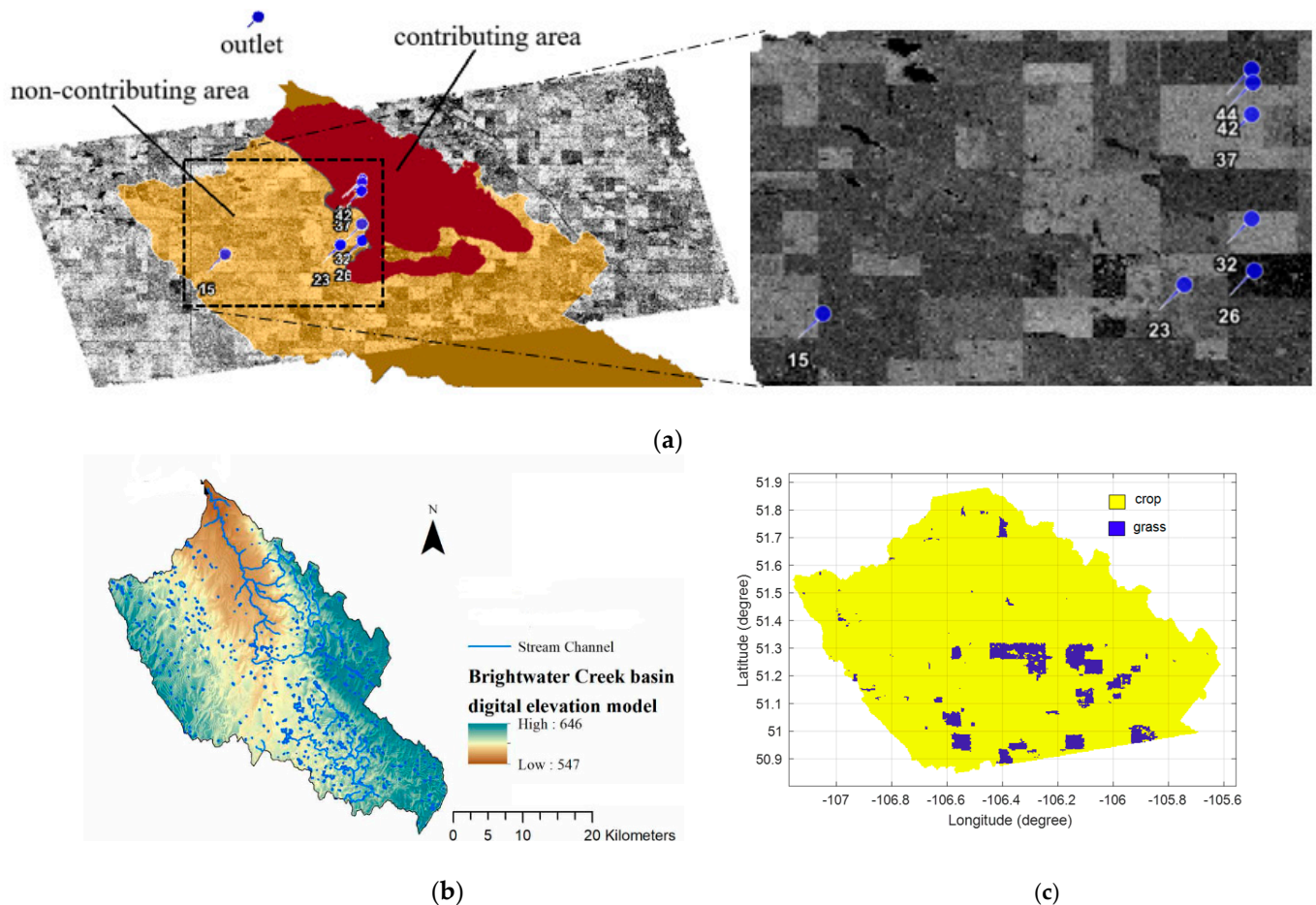
Figure 1. Bright Water Creek watershed: (**a**) local stations located in the study domain (numbers refer to the last two digits of station ID 27010XX), (**b**) DEM in meters [4] and (**c**) land cover.

Table 1. Validations for the local stations.

Station ID	Latitude (Degree)	Longitude (Degree)	Radarsat-2 Soil Moisture				SMAP Soil Moisture			
			RMSE (m³/m³)	Bias (m³/m³)	ub RMSE (m³/m³)	Retrieval Mean (m³/m³) (Field Measurements)	RMSE (m³/m³)	Bias (m³/m³)	ub RMSE (m³/m³)	Retrieval Mean (m³/m³)
2701015	51.3577	−106.573	0.06	0.05	0.04	0.26 (0.20)	0.15	−0.14	0.03	0.06
2701023	51.3679	−106.449	0.07	0.01	0.07	0.29 (0.25)	0.16	−0.14	0.07	0.13
2701026	51.3727	−106.425	0.09	−0.03	0.08	0.28 (0.28)	0.22	−0.21	0.08	0.10
2701032	51.3904	−106.426	0.06	0.03	0.05	0.25 (0.19)	0.11	−0.04	0.10	0.17
2701037	51.4262	−106.426	0.07	0.02	0.06	0.28 (0.22)	0.16	−0.13	0.09	0.11
2701042	51.437	−106.426	0.06	0.05	0.04	0.28 (0.22)	0.13	−0.12	0.07	0.11
2701044	51.4416	−106.426	0.06	0.01	0.05	0.29 (0.28)	0.18	−0.18	0.04	0.10

2.2. Field Measurements

The local stations monitor several physical variables, such as surface soil moisture and rainfall. These data were acquired from the Kenaston soil moisture network operated by the University of Guelph and Environment and Climate Change Canada [45]. The soil moisture data for the topsoil at 5 cm were collected with Hydra Probe sensors and 30-min time intervals. The rainfall data were measured with a tipping bucket rain gauge with 30-min time intervals. The soil texture varied from loam to clay loam. For this study, data for June to July in 2018 were collected.

SAR soil moisture at 100 m resolution was validated with the local stations. Due to the high resolution, a single station was considered sufficient to spatially represent each pixel without the need for an additional spatial analysis or upscaling. To evaluate the effects of rainfall on SAR retrievals, the accumulations for the rain events that occurred for 24 h before the RADARSAT-2 data acquisition were examined. The soil moisture measurements from the in situ stations were obtained at the closest time to the Radarsat-2 data acquisition.

As shown in Figure 1b, the catchment area is located at elevations of 547~646 m [7]. During the spring period, snowmelt water in certain portions of the watershed becomes overland flow that drains into channels or ponds in fields [46]. This flow empties at the riparian outlet (05HG006) operated by the Water Survey of Canada, as shown in Figure 1a. The daily water levels at the outlet were retrieved from Environment and Climate Change Canada's Historical Hydrometric Data (https://wateroffice.ec.gc.ca/report/historical_e.html?stn=05HG006) accessed on 1 March 2022. The basin outlet is located at 51°36′46″ N and 106°32′16″ W in Saskatchewan. The gross drainage area of this outlet is 1540 km^2, while the effective drainage area is 506 km^2.

As shown in Figure 1c, this catchment mostly consists of crop lands (cereals, oilseeds and pulse crop) with some patches of grasses. For the vegetation distribution illustrated in Section 3, 8-day MODIS Leaf Area Index (LAI) version 6.1 data at a resolution of 500 m was extracted from the MCD15A2H dataset [47].

2.3. Radarsat-2 Soil Moisture Retrieval Algorithm

Radarsat-2 was launched in 2007 to ameliorate ice monitoring, disaster management, resource management and mapping in various fields such as hydrology, forestry and agriculture. Fully polarized SAR backscatter data at C-land (5.4 GHz) for the period of June to July 2018 were obtained from MDA (formerly MacDonald, Dettwiler and Associates). As shown in Figure 1a, Level-1 Single Look Complex (SLC) data were obtained as fully polarized images with an approximate pixel size of 20 × 20 m. Over the study area, the temporal resolution was 3~14 days. The SAR data was imaged at a broad range of incidence angles between 22 and 43° using ascending passes obtained at 1:00 AM UTC.

For the preprocessing steps, the VV-polarized data were selected, multi-looked and projected to a ground range. After calibrating the images following Laur et al. [48], a terrain correction (Range-Doppler Terrain Correction) was performed with ESA's Sentinel Application Platform (SNAP) python tool. After co-registration, multitemporal speckle filtering (filter type: Lee Sigma, size: 7 × 7) was performed for the time series datasets [49]. Finally, the data were resampled to 100 m over the study domain shown in Figure 1a, resulting in 195,600 pixels.

2.3.1. SAR Scattering Model

SAR backscatter data were inverted to soil moisture using the lookup table (LUT) approach, which is used to computationally efficiently find an inversion solution for more than one parameter [14,21,37,50]. For the forward model, the Advanced Integral Equation Model (AIEM) was employed. It is a physically based surface scattering model that incorporates multiple scattering backscatter coefficients with inputs of the dielectric constant, surface roughness and SAR frequency. As compared to the original IEM [31,51], Advanced IEM was adjusted to incorporate multiple scattering and all the phase terms in Green's function, making more accurate calculations of the single scattering for a rough

surface. Multiple scattering considers the radiometric interactions between a surface and the medium above it, and accounts for upward and downward reradiation. In addition to a Kirchhoff term of the original IEM, cross-scattering and complementary scattering coefficients are added to this modified version: the cross term is made up of eight terms, and the complementary term has 64 terms, as described by Chen et al. [52]. A more detailed description of the AIEM is provided by the following equation.

$$\sigma_{pp}^o = \frac{k^2}{2} \exp\left[-s^2\,(\mathrm{k}_z^2 + \mathrm{k}_{sz}^2)\right] \sum_{n=1}^{\infty} s^{2n} \left|I_{\mathrm{PP}}^n\right|^2 \frac{W^n\left(k_{\mathrm{sx}} - k_{\mathrm{x}}, k_{\mathrm{sy}} - k_{\mathrm{y}}\right)}{n!} \tag{1}$$

where subscript *pp* indicates the polarization, *k* is the wave number and *S* is the standard deviation of the surface height. k_{x} is $k\sin\theta_i\cos\rho_i$, k_{y} is $k\sin\theta_i\sin\rho_i$, k_{z} is $k\cos\theta_i$, k_{sx} is $k\sin\theta_s\cos\rho_s$, k_{sy} is $k\sin\theta_s\sin\rho_s$, k_{sz} is $k\cos\theta_s$, where θ is the incidence angle and ρ is the azimuth angle, and subscript *i* for each angle is the incident angle and subscript *s* is the scattering angle. I_{PP}^n is a function of the Fresnel reflection coefficient, relative permittivity and permeability of the surface, and W^n is the Fourier transform for the nth power of the normalized surface correlation function.

The soil roughness provided as a model input for the LUT was characterized as follows. A gaussian shape was used for describing agricultural fields for the Autocorrelation Function (ACF) [32,53,54]. The Root Mean Square (RMS) height ranged from 0.2 to 4 cm, adjusted by increments of 0.1 cm. The correlation length was between 0.7 and 21.4 cm using increments of 0.3 cm. The real part of the dielectric constant was between 2.93 and 35.03 using increments of 0.03.

2.3.2. Optimization of a Cost Function

The AIEM inversion approach minimizes the cost function to retrieve soil parameters, as shown by Lee et al. [34]. From the LUT that stores the backscatter coefficient values simulated in various surface conditions, the physical parameters that produce the Radarsat-2 backscattered signals at the specified incidence angle and SAR frequency were selected. In the first step, the inversion selected RMS height [53] and correlation length values that minimized the difference between the Radarsat-2 measured and IEM model-simulated backscattering coefficients under various dielectric constant conditions [34].

As below, it minimizes the difference between Radarsat-2 measurement $\sigma_{\mathrm{Radarsat\text{-}2}}$ and IEM model-simulated backscatter coefficients σ_{IEM} under various dielectric constant and roughness conditions as follows:

$$\min\ |\sigma_{\mathrm{Radarsat\text{-}2}} - \sigma_{\mathrm{IEM}}\,(\varepsilon, \mathrm{RH})| \tag{2}$$

where σ_{IEM} is as a function of the ε dielectric constant and the RH soil roughness.

The roughness retrieved was restricted by the validity range [28].

In the second step, the inversion algorithm determined the dielectric constant value by repeating the cost minimization with the roughness retrieved from the first step.

$$\min\ |\sigma_{\mathrm{Radarsat\text{-}2}} - \sigma_{\mathrm{IEM}}\,(\varepsilon)| \tag{3}$$

Finally, the dielectric constant values from the second step were converted to soil moisture using a dielectric mixing model [55].

2.3.3. Stochastic Bias Correction

As briefly discussed in Section 1, volume scattering arising from vegetation effects in crop lands makes soil moisture retrieval complicated. The interactions between the soil surface and vegetation cover are not explicitly formulated by the currently available scattering models. In addition, it is challenging to accurately characterize vegetation structures with remote sensing data. To correct retrieval errors arising from the effects of vegetation in crop lands, we employed a stochastic method. It randomly perturbs a

poorly parameterized input variable—roughness, in this study—with a Probability Density Function (PDF) to take into account its uncertainty. When determining the parameters to be perturbed, it is assumed that the vegetation effects in crop lands have more influence on the estimation of the soil roughness than the backscattering measurement errors arising from speckle, terrain correction or calibration errors [34]. The perturbation scheme for soil roughness is as follows:

$$Z_{RH} \sim N\left(\mu_{RH}, \sigma_{RH}{}^2\right) \tag{4}$$

where Z is a set of ensembles, and subscript RH is for the roughness. N represents a normal distribution with mean μ and variance σ^2.

μ in Equation (4) is the soil roughness deterministically inverted from Radarsat-2 backscatter, as described in Section 2.3.2. These RMS height and correlation length values were stochastically perturbed with the assumption of a 50% variance, while the ensemble size was 20 [34]. Over grass lands, deterministic retrieval products were used without a stochastic bias correction. The roughness ensembles generated by Equation (4) and the original deterministic Radarsat-2 backscattering were used to produce soil moisture ensembles. The mean values of those ensemble were used as bias-corrected final products [38].

2.4. SMAP Soil Moisture

The Soil Moisture Active Passive (SMAP) radiometer operates at the L-band (1.41 GHz). Low-resolution SMAP L-band brightness temperatures were combined with high-resolution Copernicus Sentinel-1 C-band (5.404 GHz) backscatter coefficients to derive high-resolution data [56]. They were resampled to the Earth-fixed, cylindrical 3 km Equal-Area Scalable Earth Grid, Version 2.0 (EASE-Grid 2.0) [12]. Various spatial resolutions ranging from 1 to 36 km are available. Soil moisture data for the period of June to July 2018 were obtained from the NASA National Snow and Ice Data Center Distributed Active Archive Center [56]. In this study, 1 km soil moisture data from SMAP/Sentinel-1 L2 Radiometer/Radar 30 s Scene 3 km EASE-Grid Soil Moisture version 3 SMAP_L2_SM_SP_1BIWDV data were used. The temporal resolution over the study domain was 5~13 days. The orbit was descending.

3. Results

3.1. Local Validation for Time Series SAR Soil Moisture: Point Scale

Figure 2 demonstrates time series soil moisture dynamics at several stations. Because it is crop land, it was necessary to mitigate the vegetation effects, as discussed in Section 2.3.3. As shown in Table 1, the study site was usually moderately wet, showing that the time-averaged soil moisture field measurements were between 0.19 and 0.28 m^3/m^3, approximately. Similarly, bias-corrected Radarsat-2 showed 0.25~0.29 m^3/m^3 for the pixels where each local station is located. Their Root Mean Square Errors (RMSEs) were 0.06~0.09 m^3/m^3. Due to Radarsat-2 overestimation, positive biases were mostly found around 0.01~0.05 m^3/m^3, except station 2701026 at -0.03 m^3/m^3. The ubRMSEs were 0.04~0.08 m^3/m^3.

In comparison to the overestimation of Radarsat-2 retrievals, there were larger underestimations of the 1 km SMAP at all local stations. Compared to the time-averaged soil moisture total of the local stations at 0.236 m^3/m^3 and Radarsat-2 at 0.2357 m^3/m^3, the time-averaged SMAP soil moisture products were much lower at 0.112 m^3/m^3. The RMSEs of the SMAP soil moisture products were between 0.11 and 0.22 m^3/m^3. The ubRMSEs were 0.03~0.10 m^3/m^3. Negative biases were found between -0.04 and -0.21 m^3/m^3. This SMAP underestimation was consistent for all stations, regardless of rain events. These SMAP products were just pure data obtained from the website and not bias-corrected. It was previously suggested that a source of retrieval biases is thought to be related to vegetation [57–60]. Based upon Fan et al.'s research [61], SMAP soil moisture is usually underestimated in vegetated areas because of biases in the European Centre for Medium-Range Weather Forecasts (ECMWF) or the Global Modeling and Assimilation Office (GMAO) land surface temperature in vegetated areas. Singh et al. [18] also found high unbiased RMSEs of

SMAP soil moisture in paddy regions. They discussed that the imperfect radiative transfer models, as discussed above, cause vegetation-related biases, because several parameters in tau-omega models become uncertain at high vegetation water contents.
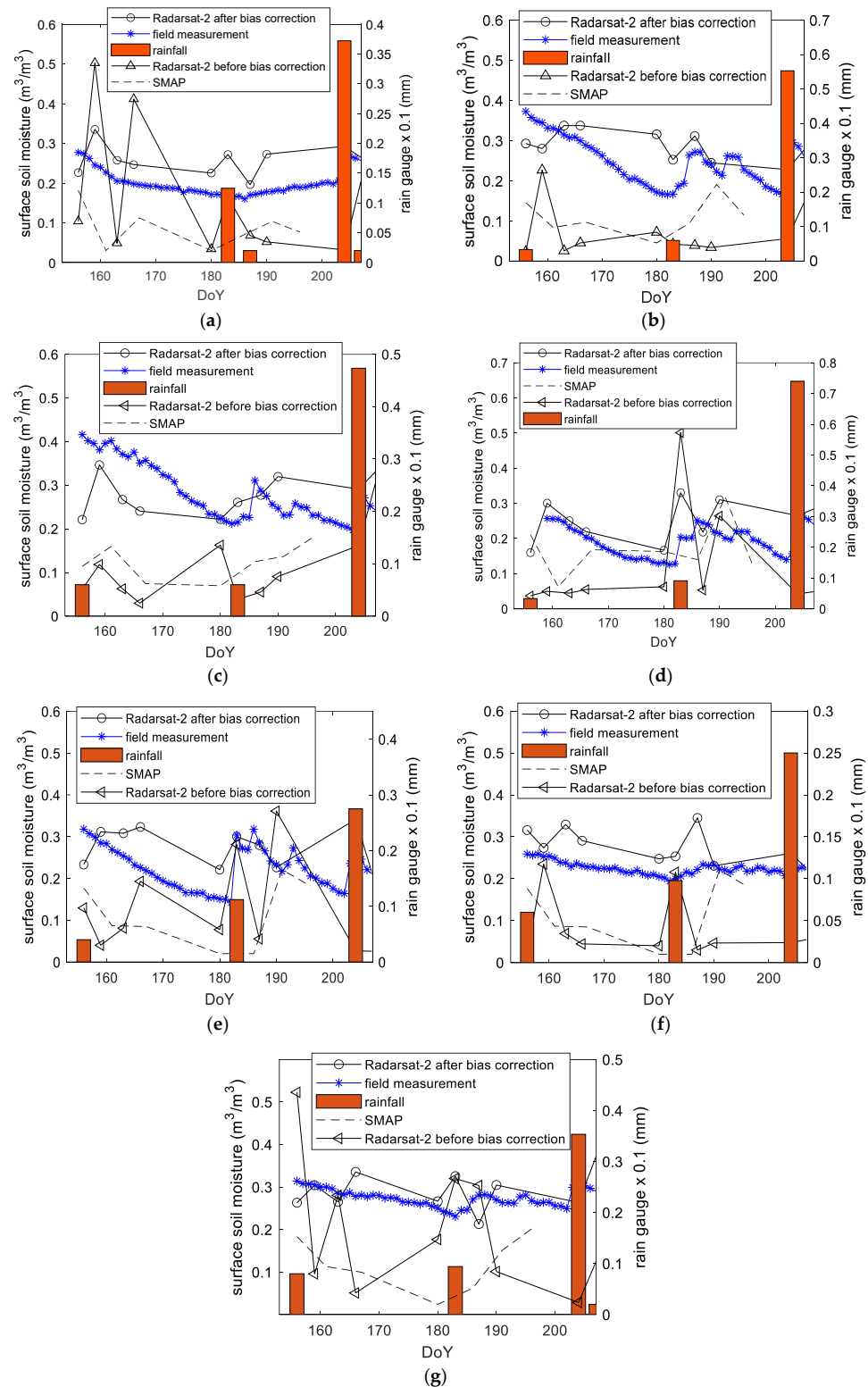
Figure 2. Validation of the soil moisture retrievals from the local stations (figures (**a**–**g**) are in the same order with Table 1).

On the other hand, for Radarsat-2, such vegetation effects are considered to be mitigated by the bias corrections made in Section 2.3.3. Accordingly, it is speculated that the RMSEs or biases of Radarsat-2 were more likely to be related to backscattering measurement or calibration errors, low-resolution soil texture information [14] or to resampling errors.

3.2. Spatial Distribution: Sub-Catchment Scale

In addition to time series validation at a point scale in Section 3.1, the same retrieval algorithm was assessed at a spatial scale and compared with the distribution of SMAP soil moisture. To illustrate its spatial responses to meteorological forcing, two hydrologically different conditions (Day of Year, DoY 156 and 190) were selected and compared. In Figure 2, the rain gauge data show that all local stations experienced rain events around DoY 182~183. Before this day, drying conditions were noticeable across the in situ network. Thus, DoY 156 was selected as the beginning of the dry-down period following a rainfall event on DoY 155. In contrast, after the rain event on DoY 182~183, the field measurements of soil moisture at all local stations reported elevated soil moisture levels. The effects of the rainfall were considered to be broad enough to cover the entire study area. Hence, DoY 190 after the rain events was selected as the wet day.

3.2.1. Dry Period Comparisons

Figure 3a shows the spatial distributions of Radarsat-2 soil moisture on DoY 156. It was moderately wet around $0.2 \text{ m}^3/\text{m}^3$ across the study domain. It was also discussed that low soil moisture areas were largely affected by land cover type, as shown in Figure 1c. Over grass lands, no stochastic retrievals were applied, because the AIEM was well conditioned to simulate multiple scattering over grass lands. Therefore, deterministic retrievals were used as described in Section 2.3.2. In contrast, SMAP soil moisture appears to be influenced by vegetation effects. In Figure 3b, SMAP showed very low soil moisture levels around $0.025 \text{ m}^3/\text{m}^3$, especially over a region with a higher LAI around $1.5 \text{ m}^2/\text{m}^2$ around 51.4 N and -106.35 W, in Figure 3c. This relationship between a high LAI and low SMAP soil moisture may be in accordance with the issues suggested by Singh et al. [18], Zwieback et al. [60] and Fan et al. [61]. Overall, SMAP soil moisture was drier at $0.1390 \text{ m}^3/\text{m}^3$ of the spatial average as compared to Radarsat-2 at $0.2758 \text{ m}^3/\text{m}^3$.

3.2.2. Wet Period Comparisons

Figure 4a shows the spatial distributions of Radarsat-2 soil moisture on DoY 190. Entire areas have elevated soil moisture levels relative to the Figure 3a, except a few patches in the grass lands. Most of areas were uniformly wet above $0.3 \text{ m}^3/\text{m}^3$. As shown in Figure 4b, the Radarsat-2 backscattered data are largely affected by land management practices, resulting in the lattice patterns, and are not associated with PFRA-contributing areas.

In contrast, the spatial patterns observed in SMAP soil moisture were comparable to PFRA hydrological classification. The PFRA-contributing areas of the watershed, as indicated by the yellow line in Figure 4c, were slightly wetter than the remaining areas. This SMAP-contributing area was thought to be determined at the early stage of the SMAP brightness temperature estimation rather than a later stage of the retrieval algorithm or land surface, such as soil texture, tillage or topography. More specifically, the high brightness temperature throughout the noncontributing area in Figure 4d matched well with the low soil moisture over the same area in Figure 4c. Thus, this appropriate differentiation between contributing and noncontributing areas was somehow related to the SMAP brightness temperature estimates. Further data will illustrate consistent estimations of the SMAP on the contributing area in Section 3.3.

However, in fact, it should be noted that there is no need for either SMAP or Radarsat-2 soil moisture to be necessarily consistent with the static contributing area suggested by PFRA hydrological classification, considering the catchment dynamics. The contributing area expands during wet periods, while it contracts during drying periods [8].
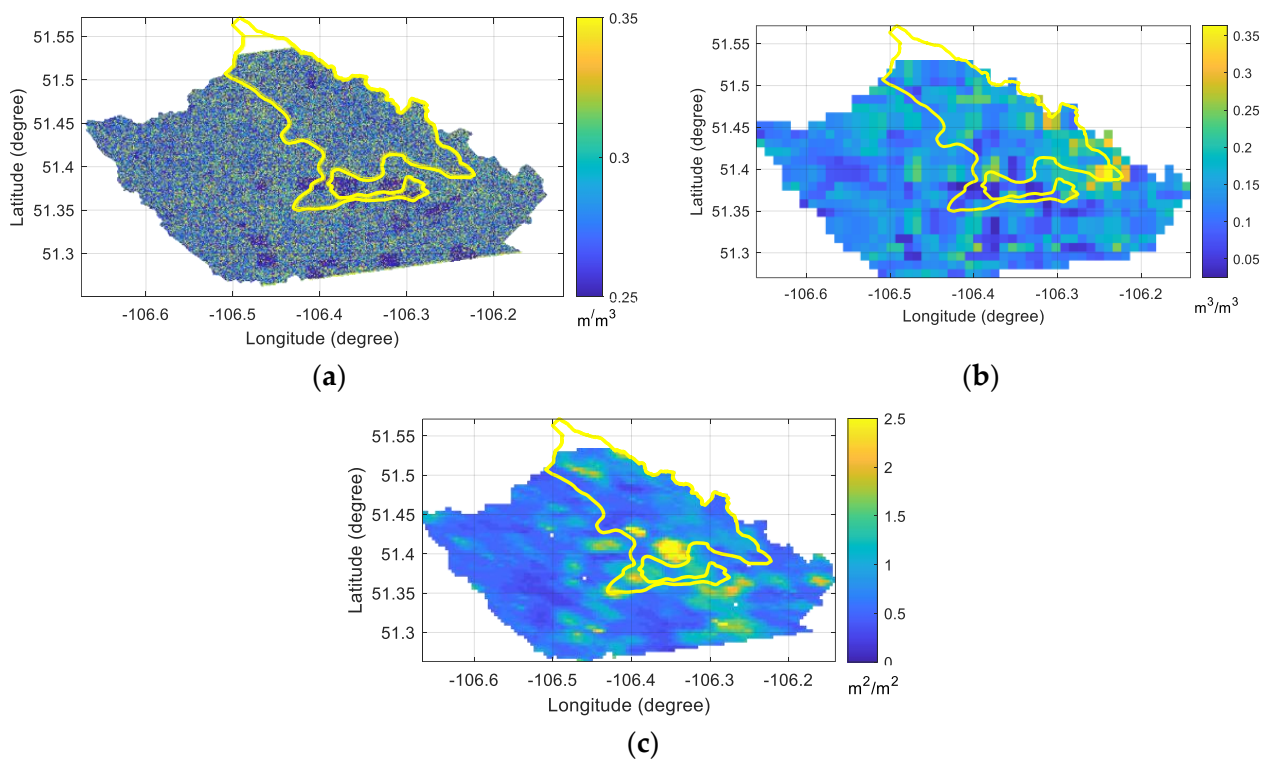
Figure 3. Spatial distribution on DoY 156: (**a**) Radarsat-2 soil moisture (m^3/m^3), (**b**) SMAP soil moisture (m^3/m^3) and (**c**) 500 m MODIS LAI on DoY 153. Contributing area is confined by the yellow line.

In terms of meteorological forcing, the SMAP did not show appropriate increases in rainfall, unlike the point data in Figure 2. More specifically, after the rain events on DoY 182~183, the SMAP decreased by 0.0143 m^3/m^3, although Radarsat-2 appropriately increased by 0.0272 m^3/m^3. In Table 2, a spatial average of Radarsat-2 soil moisture was 0.3030 m^3/m^3 on DoY 190, while the SMAP showed 0.1247 m^3/m^3 on the same day. These SMAP dry biases were also consistent with Figure 2, as well as Singh et al. [18] and Fan et al. [61]. Thus, it was suggested that Radarsat-2 responded better to meteorological forcing at this spatial scale than the SMAP. This finding is consistent with the temporal data shown in the following Section 3.3.

To sum up, the performances of Radarsat-2 and SMAP were dependent on the land surface in different ways. Although the SMAP could differentiate contributing areas from noncontributing areas at the sub-catchment scale, Radarsat-2 showed more reasonable elevations of the soil moisture with respect to meteorological forcing.

3.3. Hydrological Validation at Prairie Outlet: Watershed Scale

As compared to local stations or spatial distributions at the sub-catchment scale, much larger scale soil moisture was assessed by hydrological data at the basin outlet. The main focus of this section is to assess whether satellite-retrieved soil moisture reasonably characterizes discharge hysteresis and whether the temporal evolutions of SMAP and Radarsat-2 are sufficient for the predictions of runoff at the basin outlet in a prairie watershed [4,62].

In Figure 5, the same water level data were used for SMAP and Radarsat-2. It was found that Radarsat-2 better represented the hydrological status of watersheds, suggesting that Radarsat-2 is a better precursor of this fluctuation than the SMAP. Although the SMAP spatially better discriminated the contributing area from the noncontributing area at the sub-watershed scale in Section 3.2, its temporal evolution was not consistent with an increase in water levels at the drainage outlet.
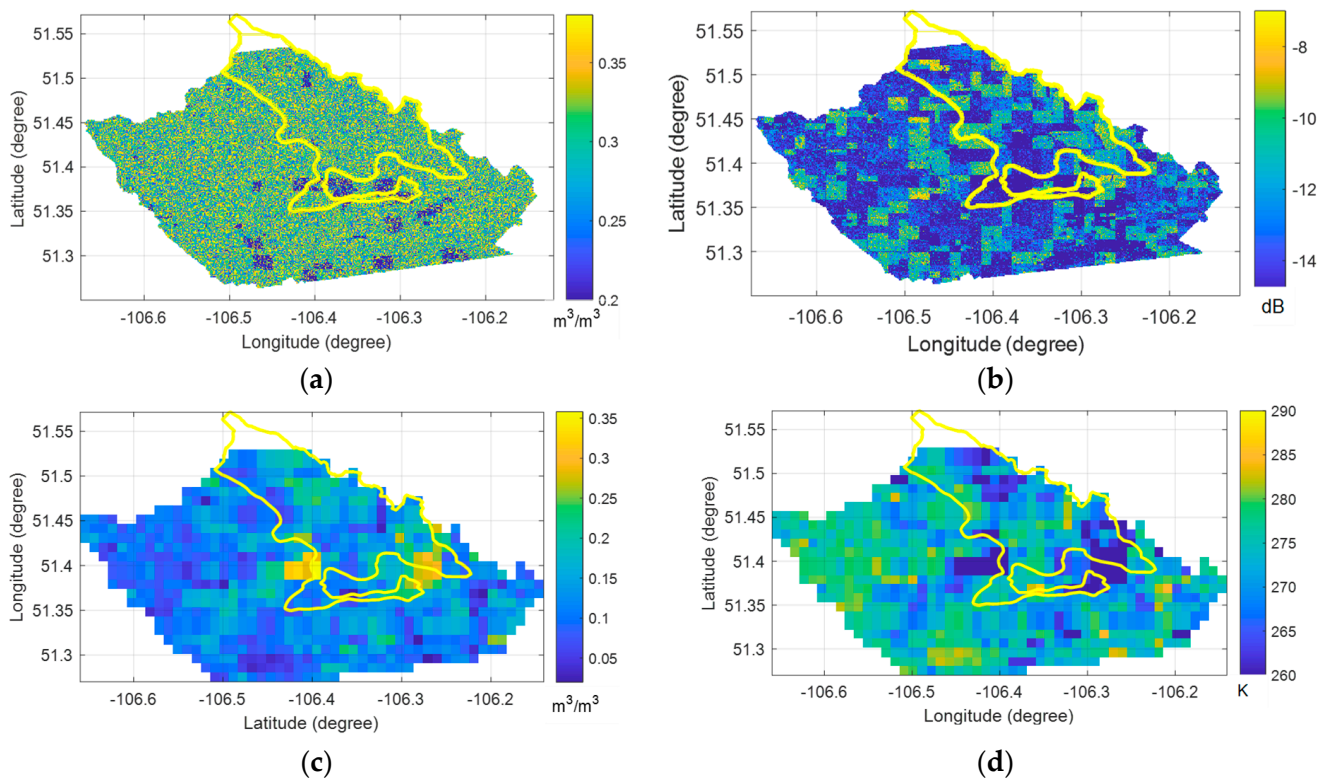
Figure 4. Spatial distribution on DoY190: (**a**) Radarsat-2 soil moisture (m^3/m^3), (**b**) Radarsat-2 backscatters, (**c**) SMAP soil moisture (m^3/m^3) and (**d**) SMAP brightness temperature. Contributing area is confined by the yellow line.

Table 2. Areal average of the soil moisture.

	Radarsat-2		SMAP	
DoY	**Backscattering Coefficient (dB)**	**Soil Moisture (m^3/m^3)**	**Brightness Temperature (K)**	**Soil Moisture (m^3/m^3)**
156	−11.5283	0.2758	261.1109	0.1390
190	−13.6557	0.3030	272.9279	0.1247

More specifically, in Figure 5, for DoY 156~178, the water levels dropped at first, then fluctuated. As Radarsat-2 decreased during DoY 159 to 162, the water levels also decreased until DoY 166. There was some time lag to reach the basin outlets downstream from the study area upstream, as shown in Figure 1a,b. When Radarsat-2 increased on DoY 165, the water levels also increased until DoY 168 (shown by 'peak 1' in Figure 5a). When Radarsat-2 decreased on DoY 179, the water levels also decreased on DoY 178. On the other hand, it was stated that SMAP soil moisture products failed to flag up a signal. The SMAP in Figure 5b continued decreasing until DoY 180, without a matched increase ('peak 1') of the water levels on DoY 168. The SMAP on DoY 180 was at the driest level around at wilting point levels (0.049 m^3/m^3). Based upon the SMAP soil moisture that consistently decreased until DoY 180 and reached the wilting point, it would not have been possible to foresee the runoff or an increase in the streamflow a few days later on DoY 183 that resulted in the highest water level ('peak 2' in Figure 5a) of 545.3 m.

In contrast, Radarsat-2 provided a better indication of increased antecedent soil water storage conditions before the same peak 2 on DoY 183 by estimating an increase in the soil moisture earlier on DoY 182. With respect to another increase in the water levels on DoY 193, it was Radarsat-2 that showed a good precursor for 'peak 3' in Figure 5a, as it estimated the increased soil moisture on DoY 189 early. In comparison, SMAP soil moisture warned about the same peak 3 days later on DoY 191.
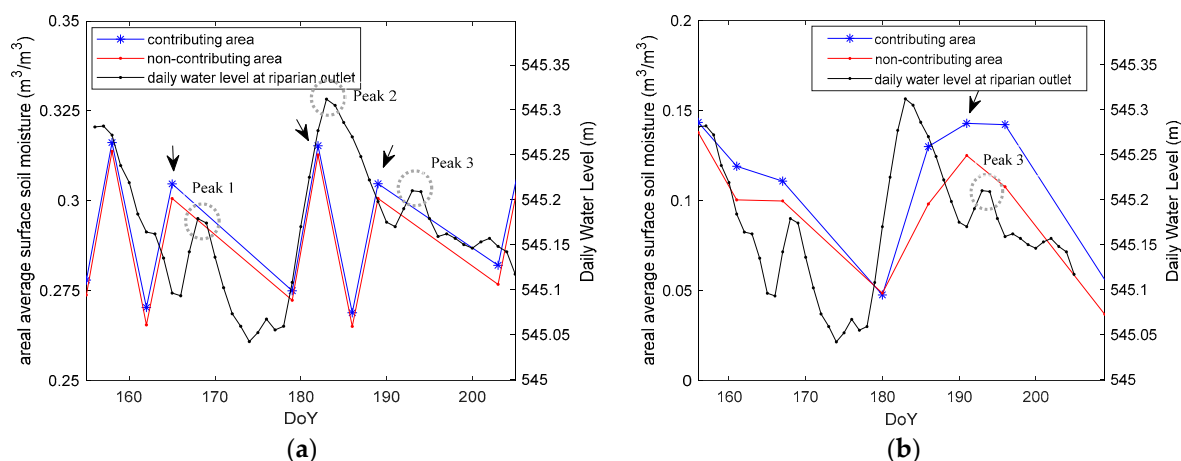
Figure 5. Areal averaged soil moisture over the contributing and noncontributing areas in comparison with the water levels at the riparian outlet: (**a**) Radarsat-2 and (**b**) SMAP.

4. Discussion

We showed that roughness-corrected Radarsat-2 soil moisture more appropriately exhibited the hysteretic dynamics of watershed storage and discharge with a time lag of 3 to 5 days, as compared to the SMAP. This finding raises several discussions in terms of timing error or hydrological (contributing area) mapping. First, temporal resolutions of Radarsat-2 soil moisture seem sufficient for capturing watershed hysteresis and hydrological dynamics, as compared to the static PFRA-contributing area mapping of SMAP soil moisture and infrequent SPOT-derived contributing area mapping (8 data for 20 months, due to clouds) [8]. Secondly, Radarsat-2 soil moisture can provide more reasonable soil water storage estimates for runoff modeling than previous studies using the NDVI or backscattering intensity used as a proxy for soil moisture. Finally, it is suggested that, based upon the comparative analysis of discharge hysteresis between the SMAP-contributing areas and Radarsat-2 soil moisture dynamics in Figure 5, reliable estimates of soil storage are more important for simulating watershed discharge than the static hydrological classification of the contributing areas.

Several caveats of each data set is discussed. The temporal resolution of 1 km SMAP soil moisture at 5~10 days was slightly lower over the study domain than Radarsat-2. Nonetheless, we had to select high-resolution data, because low-resolution SMAP had no spatial representativeness over a single local station at several cm scales in Section 3.1, and we are unable to validate the results with filed measurements in local stations. SMAP products used in this study should be comparable to a spatial resolution of Radarat-2 at 100 m. Radarsat-2 also has some limitations related to its high-spatial resolution. Although recently launched satellites tend to have higher resolutions, this does not always lead to improvements of retrievals. Several ancillary data are required to distinguish soil moisture from other physical parameters that affect satellite signals. Many of the primary ancillary datasets such as rainfall, surface temperature, VWC and soil texture are not available at the high resolution of original Radarsat-2 at 20 m or uncertain.

5. Conclusions

To apply high-resolution microwave satellite-retrieved soil moisture for improving catchment or runoff models, the effects of Radarsat-2 bias correction and SMAP soil moisture-based hydrological classification were compared at various spatial scales. To adjust the vegetation biases stemming from crop lands, a stochastic bias correction was applied for 100 m Radarsat-2 retrievals. In conjunction with 1 km SMAP soil moisture, they were validated at local stations and assessed with spatial distributions at the watershed scale (approximately 1500 km^2), as well as with water levels measured at the basin outlets.

At the point scales, Radarsat-2 had slight overestimations (positive biases: 0.01~0.05 m^3/m^3), while SMAP soil moisture showed larger underestimations (negative biases: -0.04~-0.21 m^3/m^3). The SMAP biases did not largely differ across the local stations and over time. At the sub-catchment levels, Radarsat-2 backscatters were largely affected by land cover, while LAI vegetation-related underestimations were suggested for SMAP soil moisture. Based upon consistently wet estimates of SMAP for the contributing area throughout the time in Figure 5, it was considered that SMAP distinguished PFRA-contributing areas better. On the other hand, Radarsat-2 did not show a large difference between the contributing and noncontributing areas. In relation to meteorological forcing, Radarsat-2 showed reasonably better increases in the soil moisture from rain events. At the watershed scale, Radarsat-2 soil moisture showed a better discharge hysteresis than the SMAP-contributing areas.

Based upon the results stated above, it was suggested that high-resolution Radarsat-2 soil moisture has a better hysteretic relationship with watershed discharge and can be a precursor that heralds a streamflow regime. Despite several caveats of Radarsat-2 described above, a merit of Radatsat-2 seems clear over this study site. Although some argued that decreased soil moisture variability at coarse spatial scales is more appropriate for the prediction of runoff [63], the results in this study suggest that high-resolution Radarsat-2 data reasonably well represent how soil moisture controls the streamflow regime at watershed scale and will be appropriate to use for improving runoff modeling.

Although it may be possible to better map contributing areas with microwave satellite-retrieved soil moisture, this study suggests that a reliable estimation of soil storage is more important than static classification of the contributing areas. A future work is planned to actually utilize the soil moisture products of this study for hydrological modeling.

Author Contributions: Conceptualization, J.H.L.; methodology, J.H.L.; software, J.H.L.; validation, J.H.L. and K.-E.L.; formal analysis, J.H.L. and K.-E.L.; investigation, J.H.L.; resources, K.-E.L.; data curation, J.H.L.; writing—original draft preparation, J.H.L.; writing—review and editing, J.H.L. and K.-E.L.; visualization, J.H.L.; project administration, J.H.L. and K.-E.L.; funding acquisition, K.-E.L. All authors have read and agreed to the published version of the manuscript.

Data Availability Statement: We can share Radarsat-2 soil moisture retrievals, upon request.

Conflicts of Interest: The authors declare no conflict of interest.

References

1. Brocca, L.; Melone, F.; Moramarco, T.; Wagner, W.; Naeimi, V.; Bartalis, Z.; Hasenauer, S. Improving runoff prediction through the assimilation of the ASCAT soil moisture product. *Hydrol. Earth Syst. Sci.* **2010**, *14*, 1881–1893. [CrossRef]
2. Wanders, N.; Karssenberg, D.; Bierkens, M.; Parinussa, R.; de Jeu, R.; van Dam, J.; de Jong, S. Observation uncertainty of satellite soil moisture products determined with physically-based modeling. *Remote Sens. Environ.* **2012**, *127*, 341–356. [CrossRef]
3. Massari, C.; Brocca, L.; Moramarco, T.; Tramblay, Y.; Didon Lescot, J.-F. Potential of soil moisture observations in flood modelling: Estimating initial conditions and correcting rainfall. *Adv. Water Resour.* **2014**, *74*, 44–53. [CrossRef]
4. Budhathoki, S.; Rokaya, P.; Lindenschmidt, K.-E. Improved modelling of a Prairie catchment using a progressive two-stage calibration strategy with in situ soil moisture and streamflow data. *Hydrol. Res.* **2020**, *51*, 505–520. [CrossRef]
5. Draper, C.S.; Mahfouf, J.F.; Walker, J.P. An EKF assimilation of AMSR-E soil moisture into the ISBA land surface scheme. *J. Geophys. Res. Atmos.* **2009**, *114*, D20104. [CrossRef]
6. Devia, G.K.; Ganasri, B.P.; Dwarakish, G.S. A Review on Hydrological Models. *Aquat. Procedia* **2015**, *4*, 1001–1007. [CrossRef]
7. Budhathoki, S.; Rokaya, P.; Lindenschmidt, K.-E.; Davison, B. A multi-objective calibration approach using in-situ soil moisture data for improved hydrological simulation of the Prairies. *Hydrol. Sci. J.* **2020**, *65*, 638–649. [CrossRef]
8. Mengistu, S.G.; Spence, C. Testing the ability of a semidistributed hydrological model to simulate contributing area. *Water Resour. Res.* **2016**, *52*, 4399–4415. [CrossRef]
9. Gala, T.S.; Aldred, D.A.; Carlyle, S.; Creed, I.F. Topographically based spatially averaging of SAR data improves performance of soil moisture models. *Remote Sens. Environ.* **2011**, *115*, 3507–3516. [CrossRef]

10. Gala, T.S.; Melesse, A.M. Monitoring prairie wet area with an integrated LANDSAT ETM+, RADARSAT-1 SAR and ancillary data from LIDAR. *Catena* **2012**, *95*, 12–23. [CrossRef]

11. Kerr, Y.H.; Waldteufel, P.; Richaume, P.; Wigneron, J.P.; Ferrazzoli, P.; Mahmoodi, A.; Bitar, A.A.; Cabot, F.; Gruhier, C.; Juglea, S.E.; et al. The SMOS Soil Moisture Retrieval Algorithm. *IEEE Trans. Geosci. Remote Sens.* **2012**, *50*, 1384–1403. [CrossRef]

12. Entekhabi, D.; Yueh, S.; O'Neill, P.E.; Kellogg, K.H.; Allen, A.; Bindlish, R.; Brown, M.; Chan, S.; Colliander, A.; Crow, W.T.; et al. *SMAP Handbook–Soil Moisture Active Passive: Mapping Soil Moisture and Freeze/Thaw from Space*; JPL Publication: Pasadena, CA, USA, 2014.

13. Das, N.N.; Entekhabi, D.; Dunbar, R.S.; Chaubell, M.J.; Colliander, A.; Yueh, S.; Jagdhuber, T.; Chen, F.; Crow, W.; O'Neill, P.E.; et al. The SMAP and Copernicus Sentinel 1A/B microwave active-passive high resolution surface soil moisture product. *Remote Sens. Environ.* **2019**, *233*, 111380. [CrossRef]

14. Kornelsen, K.; Coulibaly, P. Advances in soil moisture retrieval from synthetic aperture radar and hydrological applications. *J. Hydrol.* **2013**, *476*, 460–489. [CrossRef]

15. Baghdadi, N.; Aubert, M.; Zribi, M. Use of TerraSAR-X Data to Retrieve Soil Moisture Over Bare Soil Agricultural Fields. *IEEE Geosci. Remote Sens. Lett.* **2012**, *9*, 512–516. [CrossRef]

16. Gao, Y.; Gao, M.; Wang, L.; Rozenstein, O. Soil Moisture Retrieval over a Vegetation-Covered Area Using ALOS-2 L-Band Synthetic Aperture Radar Data. *Remote Sens.* **2021**, *13*, 3894. [CrossRef]

17. Zhang, L.; Meng, Q.; Yao, S.; Wang, Q.; Zeng, J.; Zhao, S.; Ma, J. Soil Moisture Retrieval from the Chinese GF-3 Satellite and Optical Data over Agricultural Fields. *Sensors* **2018**, *18*, 2675. [CrossRef]

18. Singh, G.; Das, N.N.; Panda, R.K.; Mohanty, B.P.; Entekhabi, D.; Bhattacharya, B.K. Soil Moisture Retrieval Using SMAP L-Band Radiometer and RISAT-1 C-Band SAR Data in the Paddy Dominated Tropical Region of India. *IEEE J. Sel. Top. Appl. Earth Obs. Remote Sens.* **2021**, *14*, 10644–10664. [CrossRef]

19. Attema, E.P.W.; Ulaby, F.T. Vegetation modeled as a water cloud. *Radio Sci.* **1978**, *13*, 357–364. [CrossRef]

20. Gherboudj, I.; Magagi, R.; Berg, A.A.; Toth, B. Soil moisture retrieval over agricultural fields from multi-polarized and multi-angular RADARSAT-2 SAR data. *Remote Sens. Environ.* **2011**, *115*, 33–43. [CrossRef]

21. Bindlish, R.; Barros, A.P. Multifrequency Soil Moisture Inversion from SAR Measurements with the Use of IEM. *Remote Sens. Environ.* **2000**, *71*, 67–88. [CrossRef]

22. Mirsoleimani, H.R.; Sahebi, M.R.; Baghdadi, N.; El Hajj, M. Bare Soil Surface Moisture Retrieval from Sentinel-1 SAR Data Based on the Calibrated IEM and Dubois Models Using Neural Networks. *Sensors* **2019**, *19*, 3209. [CrossRef] [PubMed]

23. Wagner, W.; Sabel, D.; Doubkova, M.; Bartsch, A.; Pathe, C. The potential of sentinel-1 for monitoring soil moisture with a high spatial resolution at global scale. In Proceedings of the Earth Observation and Water Cycle Science, Frascati, Italy, 18–20 November 2009. ESA SP-674.

24. Mattia, F.; Le Toan, T. Backscattering Properties of Multi-Scale Rough Surfaces. *J. Electromagn. Waves Appl.* **1999**, *13*, 493–527. [CrossRef]

25. Chen, K.S.; Yen, S.K.; Huang, W.P. A simple model for retrieving bare soil moisture from radar-scattering coefficients. *Remote Sens. Environ.* **1995**, *54*, 121–126. [CrossRef]

26. O'Neill, P.; Bindlish, R.; Chan, S.; Njoku, E.; Jackson, T. *SMAP Algorithm Theoretical Basis Document: Level 2 & 3 Soil Moisture (Passive) Data Products*; JPL Publication: Pasadena, CA, USA, 2015.

27. Roy, S.K.; Rowlandson, T.L.; Berg, A.A.; Champagne, C.; Adams, J.R. Impact of sub-pixel heterogeneity on modelled brightness temperature for an agricultural region. *Int. J. Appl. Earth Obs. Geoinf.* **2016**, *45*, 212–220. [CrossRef]

28. Baghdadi, N.; Gherboudj, I.; Zribi, M.; Sahebi, M.; King, C.; Bonn, F. Semi-empirical calibration of the IEM backscattering model using radar images and moisture and roughness field measurements. *Int. J. Remote Sens.* **2004**, *25*, 3593–3623. [CrossRef]

29. Merzouki, A.; McNairn, H.; Pacheco, A. Mapping Soil Moisture Using RADARSAT-2 Data and Local Autocorrelation Statistics. *IEEE J. Sel. Top. Appl. Earth Obs. Remote Sens.* **2011**, *4*, 128–137. [CrossRef]

30. Pauwels, V.R.N.; Hoeben, R.; Verhoest, N.E.C.; De Troch, F.P.; Troch, P.A. Improvement of TOPLATS-based discharge predictions through assimilation of ERS-based remotely sensed soil moisture values. *Hydrol. Process.* **2002**, *16*, 995–1013. [CrossRef]

31. Shi, J.C.; Wang, J.; Hsu, A.Y.; Neill, P.E.O.; Engman, E.T. Estimation of bare surface soil moisture and surface roughness parameter using L-band SAR image data. *IEEE Trans. Geosci. Remote Sens.* **1997**, *35*, 1254–1266. [CrossRef]

32. van der Velde, R.; Su, Z.; van Oevelen, P.; Wen, J.; Ma, Y.; Salama, M.S. Soil moisture mapping over the central part of the Tibetan Plateau using a series of ASAR WS images. *Remote Sens. Environ.* **2012**, *120*, 175–187. [CrossRef]

33. Verhoest, N.E.C.; De Baets, B.; Mattia, F.; Satalino, G.; Lucau, C.; Defourny, P. A possibilistic approach to soil moisture retrieval from ERS synthetic aperture radar backscattering under soil roughness uncertainty. *Water Resour. Res.* **2007**, *43*, W07435. [CrossRef]

34. Lee, J.H.; Budhathoki, S.; Lindenschmidt, K.-E. Stochastic bias correction for RADARSAT-2 soil moisture retrieved over vegetated areas. *Geocarto Int.* **2021**, *37*, 9190–9203. [CrossRef]

35. Zhu, L.; Walker, J.P.; Shen, X. Stochastic ensemble methods for multi-SAR-mission soil moisture retrieval. *Remote Sens. Environ.* **2020**, *251*, 112099. [CrossRef]

36. Pierdicca, N.; Pulvirenti, L.; Bignami, C. Soil moisture estimation over vegetated terrains using multitemporal remote sensing data. *Remote Sens. Environ.* **2010**, *114*, 440–448. [CrossRef]

37. Notarnicola, C.; Angiulli, M.; Posa, F. Use of radar and optical remotely sensed data for soil moisture retrieval over vegetated areas. *IEEE Trans. Geosci. Remote Sens.* **2006**, *44*, 925–935. [CrossRef]

38. Lee, J.H.; Ahn, C.K. Stochastic relaxation of nonlinear soil moisture ocean salinity (SMOS) soil moisture retrieval errors with maximal Lyapunov exponent optimization. *Nonlinear Dyn.* **2019**, *95*, 653–667. [CrossRef]
39. Lee, J.H. Using Ranked Probability Skill Score (RPSS) as Nonlocal Root-Mean-Square Errors (RMSEs) for Mitigating Wet Bias of Soil Moisture Ocean Salinity (SMOS) Soil Moisture. *Photogramm. Eng. Remote Sens.* **2020**, *86*, 91–98. [CrossRef]
40. Reichle, R.H.; Koster, R.D. Bias reduction in short records of satellite soil moisture. *Geophys. Res. Lett.* **2004**, *31*, L19501. [CrossRef]
41. Chen, F.; Crow, W.T.; Bindlish, R.; Colliander, A.; Burgin, M.S.; Asanuma, J.; Aida, K. Global-scale evaluation of SMAP, SMOS and ASCAT soil moisture products using triple collocation. *Remote Sens. Environ.* **2018**, *214*, 1–13. [CrossRef]
42. Lee, H.J.; Im, J. A Novel Bias Correction Method for Soil Moisture and Ocean Salinity (SMOS) Soil Moisture: Retrieval Ensembles. *Remote Sens.* **2015**, *7*, 5824. [CrossRef]
43. DeBeer, C.M.; Wheater, H.S.; Pomeroy, J.W.; Barr, A.G.; Baltzer, J.L.; Johnstone, J.F.; Turetsky, M.R.; Stewart, R.E.; Hayashi, M.; van der Kamp, G.; et al. Summary and synthesis of Changing Cold Regions Network (CCRN) research in the interior of western Canada—Part 2: Future change in cryosphere, vegetation, and hydrology. *Hydrol. Earth Syst. Sci.* **2021**, *25*, 1849–1882. [CrossRef]
44. Magagi, R.; Berg, A.A.; Goita, K.; Belair, S.; Jackson, T.J.; Toth, B.; Walker, A.; McNairn, H.; Neill, P.E.O.; Moghaddam, M.; et al. Canadian Experiment for Soil Moisture in 2010 (CanEx-SM10): Overview and Preliminary Results. *IEEE Trans. Geosci. Remote Sens.* **2013**, *51*, 347–363. [CrossRef]
45. Tetlock, E.; Toth, B.; Berg, A.; Rowlandson, T.; Ambadan, J.T. An 11-year (2007–2017) soil moisture and precipitation dataset from the Kenaston Network in the Brightwater Creek basin, Saskatchewan, Canada. *ESSD* **2019**, *11*, 787–796. [CrossRef]
46. Shook, K.; Papalexiou, S.; Pomeroy, J.W. Quantifying the effects of Prairie depressional storage complexes on drainage basin connectivity. *J. Hydrol.* **2021**, *593*, 125846. [CrossRef]
47. Myneni, R.; Knyazikhin, Y.; Park, T. *MCD15A2H MODIS/Terra+Aqua Leaf Area Index/FPAR 8-day L4 Global 500m SIN Grid V006*; United States Geological Survey: Reston, VA, USA, 2015.
48. Laur, H.; Bally, P.; Meadows, P.; Sanchez, J.; Schaettler, B.; Lopinto, E.; Esteban, D. Derivation of the backscattering coefficient in ESA ERS SAR PRI products. In *ESA Document No. ES-TN-RS-PM-HL09*; Revision 5f; European Space Agency: Paris, France, 2004.
49. Al-Zuhairi, M.; Nahhas, F.; Hussein, F.; Pradhan, B.; Shariff, R. A refined classification approach by integrating Landsat Operational Land Imager (OLI) and RADARSAT-2 imagery for land-use and land-cover mapping in a tropical area. *Int. J. Remote Sens.* **2016**, *37*, 2358–2375. [CrossRef]
50. Weeks, R.; Smith, M.; Pak, K.; Gillespie, A. Inversions of SIR-C and AIRSAR data for the roughness of geological surfaces. *Remote Sens. Environ.* **1997**, *59*, 383–396. [CrossRef]
51. Ulaby, F.; Moore, R.; Fung, A. *Microwave Remote Sensing: Active and Passive. Volume 2-Radar Remote Sensing and Surface Scattering and Emission Theory*; Artech House: London, UK, 1982.
52. Chen, K.S.; Tzong-Dar, W.; Leung, T.; Qin, L.; Jiancheng, S.; Fung, A.K. Emission of rough surfaces calculated by the integral equation method with comparison to three-dimensional moment method simulations. *IEEE Trans. Geosci. Remote Sens.* **2003**, *41*, 90–101. [CrossRef]
53. Davidson, M.W.J.; Thuy Le, T.; Mattia, F.; Satalino, G.; Manninen, T.; Borgeaud, M. On the characterization of agricultural soil roughness for radar remote sensing studies. *IEEE Trans. Geosci. Remote Sens.* **2000**, *38*, 630–640. [CrossRef]
54. Fung, A.K. *Microwave Scattering and Emission Models and Their Applications*; Artech House: Norwood, MA, USA, 1994.
55. Hallikainen, M.T.; Ulaby, F.T.; Dobson, M.C.; El-Rayes, M.A.; Wu, L. Microwave Dielectric Behavior of Wet Soil-Part 1: Empirical Models and Experimental Observations. *IEEE Trans. Geosci. Remote Sens.* **1985**, *GE-23*, 25–34. [CrossRef]
56. Das, N.; Entekhabi, D.; Dunbar, R.S.; Kim, S.; Yueh, S.; Colliander, A.; O'Neill, P.E.; Jackson, T.; Jagdhuber, T.; Chen, F.; et al. *SMAP/Sentinel-1 L2 Radiometer/Radar 30-Second Scene 3 km EASE-Grid Soil Moisture, Version 3*; NASA: Washington, DC, USA, 2020. [CrossRef]
57. de Jeu, R.A.M.; Wagner, W.; Holmes, T.R.H.; Dolman, A.J.; van de Giesen, N.C.; Friesen, J. Global Soil Moisture Patterns Observed by Space Borne Microwave Radiometers and Scatterometers. *Surv. Geophys.* **2008**, *29*, 399–420. [CrossRef]
58. Dorigo, W.A.; Scipal, K.; Parinussa, R.M.; Liu, Y.Y.; Wagner, W.; de Jeu, R.A.M.; Naeimi, V. Error characterisation of global active and passive microwave soil moisture datasets. *Hydrol. Earth Syst. Sci.* **2010**, *14*, 2605–2616. [CrossRef]
59. Parinussa, R.M.; Meesters, A.G.C.A.; Liu, Y.Y.; Dorigo, W.; Wagner, W.; Jeu, R.A.M.d. Error Estimates for Near-Real-Time Satellite Soil Moisture as Derived From the Land Parameter Retrieval Model. *IEEE Geosci. Remote Sens. Lett.* **2011**, *8*, 779–783. [CrossRef]
60. Zwieback, S.; Colliander, A.; Cosh, M.H.; Martínez-Fernández, J.; McNairn, H.; Starks, P.J.; Thibeault, M.; Berg, A. Estimating time-dependent vegetation biases in the SMAP soil moisture product. *Hydrol. Earth Syst. Sci.* **2018**, *22*, 4473–4489. [CrossRef]
61. Fan, X.; Liu, Y.; Gan, G.; Wu, G. SMAP underestimates soil moisture in vegetation-disturbed areas primarily as a result of biased surface temperature data. *Remote Sens. Environ.* **2020**, *247*, 111914. [CrossRef]
62. Wadsworth, E.; Champagne, C.; Berg, A.A. Evaluating the utility of remotely sensed soil moisture for the characterization of runoff response over Canadian watersheds. *Can. Water Resour. J./Rev. Can. Des Ressour. Hydr.* **2020**, *45*, 77–89. [CrossRef]
63. Álvarez-Mozos, J.; Casalí, J.; González-Audícana, M.; Verhoest, N.E.C. Correlation between Ground Measured Soil Moisture and RADARSAT-1 derived Backscattering Coefficient over an Agricultural Catchment of Navarre (North of Spain). *Biosyst. Eng.* **2005**, *92*, 119–133. [CrossRef]